Anisotropy of dose contributions—An instrument to upgrade real time IMRT and VMAT adaptation?

Klaus Bratengeier[a] and Kostyantyn Holubyev
Department of Radiation Oncology, University of Würzburg, Josef-Schneider-Str. 11, Würzburg 97080, Germany

(Received 25 February 2016; revised 13 September 2016; accepted for publication 18 September 2016; published 5 October 2016)

Purpose: To suggest a definition of dose deposition anisotropy for the purpose of *ad hoc* adaptation of intensity modulated arc therapy (IMRT) and volumetric arc therapy (VMAT), particularly in the vicinity of important organs at risk (OAR), also for large deformations.
Methods: Beam's-eye-view (BEV) based fluence warping is a standard adaptation method with disadvantages for strongly varying OAR shapes. 2-Step-adaptation overcomes these difficulties by a deeper analysis of the 3D properties of adaptation processes, but requires separate arcs for every OAR to spare, which makes it impractical for cases with multiple OARs. The authors aim to extend the 2-Step method to arbitrary intensity modulated plan by analyzing the anisotropy of dose contributions. Anisotropy was defined as a second term of Fourier transformation of gantry angle dependent dose contributions. For a cylindrical planning target volume (PTV) surrounding an OAR of varying diameter, the anisotropy and the dose-normalized anisotropy were analyzed for several scenarios of optimized fluence distributions. 2-Step adaptation to decreasing and increasing OAR diameter was performed, and compared to a usual fluence based adaptation method. For two clinical cases, prostate and neck, the VMAT was generated and the behavior of anisotropy was qualitatively explored for deformed organs at risk.
Results: Dose contribution anisotropy in the PTV peaks around nearby OARs. The thickness of the "anisotropy wall" around OAR increases for increasing OAR radius, as also does the width of 2-Step dose saturating fluence peak adjacent to the OAR [K. Bratengeier *et al.*, "A comparison between 2-Step IMRT and conventional IMRT planning," Radiother. Oncol. **84**, 298–306 (2007)]. Different optimized beam fluence profiles resulted in comparable radial dependence of normalized anisotropy. As predicted, even for patient cases, anisotropy was inflated even more than increasing diameters of OAR.
Conclusions: For cylindrically symmetric cases, the dose distribution anisotropy defined in the present work implicitly contains adaptation-relevant information about 3D relationships between PTV and OAR and degree of OAR sparing. For more complex realistic cases, it shows the predicted behavior qualitatively. The authors claim to have found a first component for advancing a 2-Step adaptation to a universal adaptation algorithm based on the BEV projection of the dose anisotropy. Further planning studies to explore the potential of anisotropy for adaptation algorithms using phantoms and clinical cases of differing complexity will follow. *© 2016 Author(s). All article content, except where otherwise noted, is licensed under a Creative Commons Attribution 3.0 Unported License.* [http://dx.doi.org/10.1118/1.4963806]

Key words: radiotherapy, adaptation, IMRT, IMAT, VMAT

1. INTRODUCTION

Real time or "*ad hoc*" adaptation of volumetric arc therapy (VMAT) or intensity modulated arc therapy (IMRT) are topics of increasing interest, as image guided radiotherapy (IGRT) is available on the radiation table. Repositioning (i.e., Wilbert *et al.*[2]) and aperture tracking (i.e., Ravkilde *et al.*)[3] are the simplest and widely used methods. Several methods are developed to provide smooth adaptation to deformed planning target volumes (PTV) and organs at risk (OAR): Fast optimization (i.e., Men *et al.*)[4] using parallel computing, re-optimization (Wu *et al.*),[5] dose or fluence deforming algorithms (i.e., Mohan *et al.*).[6] The latter are employed for prostate patients using markers (Crijns *et al.*).[7]

Nevertheless, beam's-eye-view (BEV) based methods, which warp the fluence grid along with the projected contour shapes, have a disadvantage: warping to the changed OAR diameter may under- or over-dose the PTV, as increased (decreased) OAR radius needs more (less) pronounced OAR-tangential irradiation than suggested by simple BEV warping (Bratengeier *et al.*).[8]

The authors published a "2-Step" method that avoids this effect. 2-Step constructs segments that on the one hand allow fully adequate IMRT (Ref. 1) and an intensity modulated arc technique (IMAT).[9,10] On the other hand these techniques are adaptable, putting more emphasis to the PTV adjacent to the OAR. Its capabilities are demonstrated for IMRT (Refs. 11 and 12) and an IMAT (Ref. 13) similar to VMAT,

both for sophisticated prostate cases. Special segments are created tangential to the OAR that follow their own adaptation rules avoiding the problems of fluence warping methods.[8] However, 2-Step method has its own drawbacks: The number of segments and the number of arcs, respectively, increase linearly or even hyperlinearly with the number of OARs to be considered. Consequently, 2-Step plans entail longer delivery times than normal VMAT and become impractical for the cases with multiple OARs. Also, 2-Step plan generation ignores OAR interdependence. Both the restrictions of usual fluence warping and of the 2-Step adaptation motivated the authors to develop a method that avoids the disadvantages of both.

The purpose of this work is to enhance BEV warping methods with an indicator that includes relevant 3D-information to control adaptation of tangential-to-OAR segments. Two properties are needed to ensure the applicability of the algorithm to arbitrary IMRT and VMAT plans:

- For many-field IMRT and particularly for VMAT, it is not clear from the outset, which parts of segments play the role of tangential-to-OAR dose increasers, as it is demonstrated in Fig. 1. Therefore, special 2-Step plans had to be generated in previous studies; different segment types were constructed with their specific adaptation rules. Now, the indicator should identify the specific parts of each segment that need special adaptation rules, especially for the near-OAR areas. The algorithms should be applicable also for segments of mixed nature that were not primarily assigned a special role.
- Second, the adaption of the indicator itself should drive the adaptation of the segments. In other words, for changed PTV-OAR geometry, the indicator should behave similar to the width of the special 2-Step segments required to saturate the dose around the OAR: it should increase for increasing OAR diameter and to decrease otherwise (even in a disproportional way, as we will see in Sec. 2.C).

The authors introduce a measure of dose anisotropy as such an indicator. They present several properties of their definition of anisotropy and demonstrate the relevance for the adaptation problem for the situation of a PTV-encompassed OAR as it was used by Brahme *et al.*[14] Also some examples will be discussed.

Based on these considerations the authors aim to pave the way for a procedure similar to that described in the following:

(1) Based on a primary CT with OAR and PTV structures, an IMRT or VMAT plan is optimized. No special method would be required for planning or optimization. The related anisotropy vector field has to be calculated together with the projection of the vectors in the BEV and their relation to the beams segments and structures.
(2) The daily target and the daily OARs have to be contoured in the actual cone beam computed tomography (CBCT) or MR using fast algorithms or special contouring tools. The anisotropy is then warped in 3D and the BEV projections of structures along with the BEV projections of anisotropy vectors are calculated to adapt the beam shapes.
(3) The MU-conserving plan can be examined using simple plausibility checks. Dose accumulation and potentially dose corrections from the accumulation are applied.

2. METHODS

2.A. An anisotropy definition

In the 2-Step IMRT/IMAT adaptation, the purely tangential second order segments (leaf openings) saturate the "shadowed" PTV areas adjacent to the OAR. These leaf openings follow special adaptation rules diverging from simple warping[8] (see Sec. 2.C). We introduce anisotropy to identify such "second order" ($S2$)-type leaf openings. Intuitively, we need an anisotropy definition which reaches its maximum for a single field and vanishes for isotropic irradiation. A definition

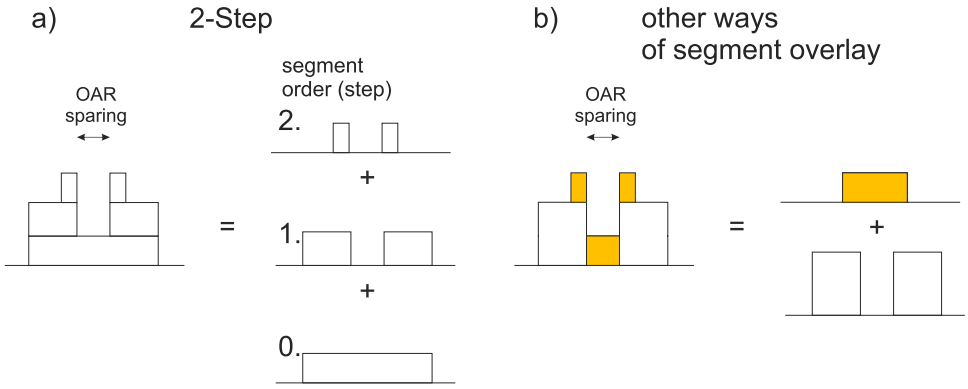

FIG. 1. (a) Segments for dose sparing of OAR according to the 2-Step-technique without PTV underdosage. (b) Similar effect resulting from a common IMRT optimization technique.

of anisotropy which fulfils these requirements is

$$\vec{A}_k := \sum_i \vec{A}_{ik} = \sum_i D_{ik} \begin{pmatrix} \sin 2\gamma_i \\ \cos 2\gamma_i \end{pmatrix}, \tag{1}$$

$$\vec{A}_{k,n} := \frac{\sum_i \vec{A}_{ik}}{\sum_i D_{ik}} \text{ for } \sum_i D_{ik} \neq 0, \tag{2}$$

with an un-normalized variant $\vec{A}$ and a normalized variant $\vec{A}_n$. The dose contribution D_{ik} at the voxel k results from the field i at gantry angle γ_i. This definition applies to any form of IMRT and VMAT.

In reality, always $\sum_i D_{ik} \neq 0$. For the idealized case, we define $\vec{A}_{k,n} := 0$ for $\sum_i D_{ik} = 0$. Note that the underlying vector space $\vec{A}$ is not identical to a normal 3D space or a 2D subspace; it is rather part of a phase space, with components of $\vec{A}$ corresponding to the Fourier-coefficients a_2 and b_2.

The absolute value of vector $\vec{A}$ is the measure of anisotropy

$$A = \left|\vec{A}\right|. \tag{3}$$

For pure opposing fields or a single field, especially for tangential irradiation, the maximal value for normalized anisotropy strength of $\left|\vec{A}_n\right| = 1$ can be reached; otherwise $\left|\vec{A}_n\right| < 1$. For superposition of equi-weighted orthogonal segments or the special situation of isotropic irradiation $A = 0$ is obtained.

The "effective direction" γ is of interest. It results from all directions of irradiation, and can be computed from the components of the vector $\vec{A}$,

$$\gamma := \begin{cases} \frac{1}{2}\tan^{-1}\left(\frac{\sum_i D_i \sin 2\gamma_i}{\sum_i D_i \cos 2\gamma_i}\right) \\ \\ \frac{\pi}{4} \end{cases} \text{ for } \sum_i D_i \cos 2\gamma_i \begin{cases} \neq 0 \\ = 0 \end{cases}. \tag{4}$$

For a single field, γ represents its irradiation angle or the opposite one.

Figure 2 illustrates anisotropy in the case of a PTV surrounded by an OAR that is to be optimally spared. Whereas at point P', far away from the OAR, the dose is allowed to sum up from all directions isotropically, at P'' the dose can only be contributed from directions tangential to OAR. In the first case P', the anisotropy and normalized anisotropy both approach zero, in the second case P'', the anisotropy must approach its maximal value (roughly equals the dose), and normalized anisotropy approaches unity. The intermediate point P is chosen in a way that the range α of allowed angles of incidence, which spare the OAR, is the half of the full angle. If the dose is evenly distributed within α, normalized anisotropy is 0.5.

2.B. Examples (simple beam model and geometry)

A standard situation was chosen to evaluate the anisotropy function: a cylindrical OAR surrounded by a hollow-cylindrical PTV. The outer PTV cylinder had a normalized

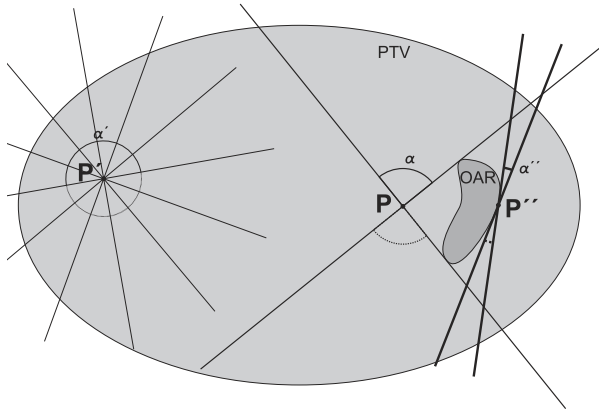

FIG. 2. Considerations on anisotropy at points P, P', P'' for an OAR within or nearby the PTV.

radius of 1, its inner border could be adjacent to the OAR with or without a gap. The simplified approach ignored divergence, absorption, and scatter—it was purely "geometrical." For this approach, Brahme's solution[14] exists, an intense fluence peak adjacent to the OAR according to the radial fluence distribution

$$d(r) = \frac{d_0}{\sqrt{1 - \frac{R_{\text{OAR}}^2}{r^2}}} \tag{5}$$

that creates a completely homogeneous dose distribution throughout the PTV, while rotating 360°. The 2-Step solution approximated this function by a homogeneous fluence covering PTV but blocking out the OAR ("first step" $S1$, Fig. 1) and a "second step" segment ($S2$, also called second order), a rotating narrow segment tangential to the OAR with optimized weight and width[15] to approximate Brahme peak. As the problem is scale-invariant, all distances were normalized to R_{PTV}, the outer radius of the PTV. For 2-Step, two beam models were chosen: One idealized "geometric," neglecting scatter and divergence, with rectangular beam profile. To analyze the behavior of normalized anisotropy, with its small denominator, a more sophisticated beam model with partially small dose contributions was needed. Therefore, a symmetric (isosceles) trapezoid beam profile, as a simple approximation of electron scatter and effects of finite beam focus was additionally used. The penumbra was defined as the 20%–80% isodose distance. Beam width was defined as the half width of the profile. Also, an anisotropic dose contribution was assumed to model photon scatter and any isotropic background.

2.C. Relation to adaptation schemes (simple beam model and geometry)

For adaptation purposes, OAR was assumed to inflate and to shrink. The adaptation rules similar to intensity warp in BEV (Ref. 6) and the 2-Step based method[8] were applied. Radial dose distribution, anisotropy, and normalized anisotropy were compared.

Widths of ($S2$-) segments to compensate underdosage due to OAR sparing were corrected by

$$\Delta S2 = \Delta R_{\mathrm{OAR}} \times \mathrm{DC} \quad (6)$$

depending on the changes ΔR_{OAR} of the OAR-radius.[8] The differential coefficient DC was determined from the phantom studies. DC = 0 leads to a segment width deformation proportional to the changes of the OAR radius. DC < 0 for a minor increase of segment width for increasing OAR radius and DC > 0 characterizing disproportionate increase of segment width. According to phantom planning studies, necessary DC always was >0 (typically between 0.5 for large OAR radii with respect to the PTV diameter and 1.5 for small radii) as it is demanded by theory for the 2-Step adaptation algorithm. That means, for OAR inflation the 2-Step method correctly predicts additional necessary dose contribution in the vicinity of inflated OAR. For warping methods DC was always <0; the PTV in the vicinity of the OAR will be underdosed.

It should be investigated whether anisotropy can be used to describe qualitatively or even quantitatively the necessary changes of additional tangential dose contributions (vice versa overdosed for shrinking OAR).

2.D. Examples (realistic beam, patient model, and plans)

In contrast to the quantitative considerations in the latter two paragraphs, this group of examples illustrates the potential of anisotropy concept for real clinical VMATs. The sophisticated VMAT plans were optimized for prostate and head and neck cases. Then OAR shapes were systematically changed based on the original CT, and the VMATs were reoptimized to the changed geometry. The absolute anisotropy $|\vec{A}|$ was calculated according to Eq. (1) and depicted for some slices.

For the prostate case, rectum was virtually inflated by 5 mm in lateral direction to both sides. In a second variant, rectum was additionally inflated by 5 mm in ventral direction. In the head and neck case, the right parotid was inflated in ventro-dorsal and lateral direction by 10 mm. Also, the gap between the two parts of caudal lymph drainage areas was increased. The reoptimization to deformed OARs was performed with the same sets of objectives; the nominal weights were increased by the ratio of the volumes of deformed and original OARs to ensure the same weight per voxel. For adaptation and dose calculation, a Philips PINNACLE3 planning system (V9.10) was used. Anisotropy was calculated according to Eq. (1) externally from the exported DICOM RT-Dose and RT-Plan and read back into PINNACLE3.

3. RESULTS

3.A. Anisotropy for different optimized fluence distributions

For Brahme and 2-Step fluence, three OAR-radii were chosen as examples: $R_{\mathrm{OAR}} = 0.1$, 0.25, and 0.6 for a zero-gap between OAR and PTV. 2-Step was also applied for gaps of 0.05 and 0.10 besides a zero-gap. From earlier work on 2-Step method[15] follows that the pair [radius of OAR R_{OAR}; gap width] translates into → [segment width; segment weight] for the narrow second step segments $S2$
[0.10;0.00] → [0.026;2.32], [0.10;0.05] → [0.095;0.62], [0.10;0.10] → [0.147; 0.37],

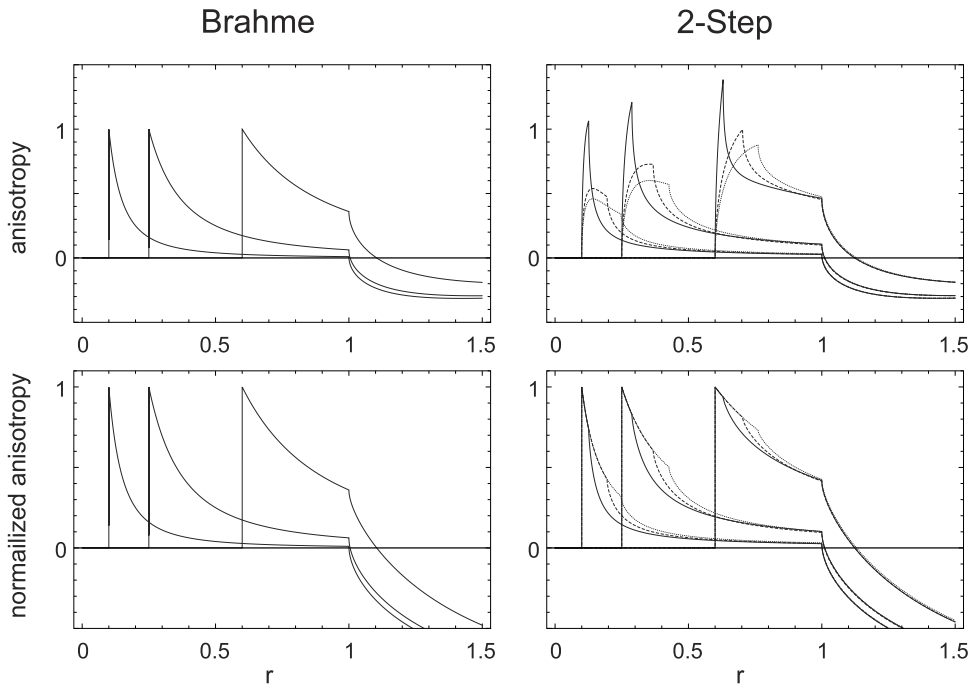

FIG. 3. Anisotropy and normalized anisotropy for Brahme (left) and 2-Step (right) solutions, depending on distance r from the OAR-center, normalized to the PTV-radius. OAR-radii: 0.1, 0.25, and 0.6. Solid line: no gap between OAR and PTV; dashed and dotted line: gap width 0.05 and 0.1, respectively. Upper row: anisotropy; lower row: normalized anisotropy.

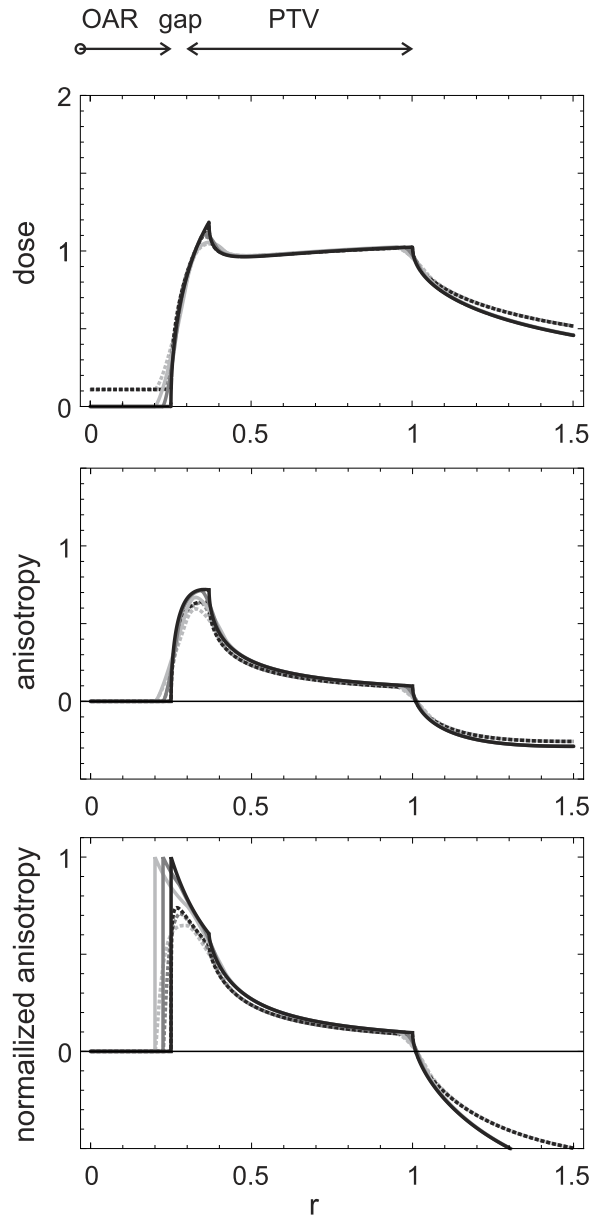

FIG. 4. Influence of beam profile and isotropic background on anisotropy. $R_{OAR} = 0.25$, gap width 0.05, $R_{PTV} = 1.00$. Black solid line: rectangular profile. Dark grey and light grey lines: trapezoidal profile with penumbra 0.03 and 0.06, respectively. Dotted lines: additional dose background by isotropic contributions: 10% of PTV plateau dose.

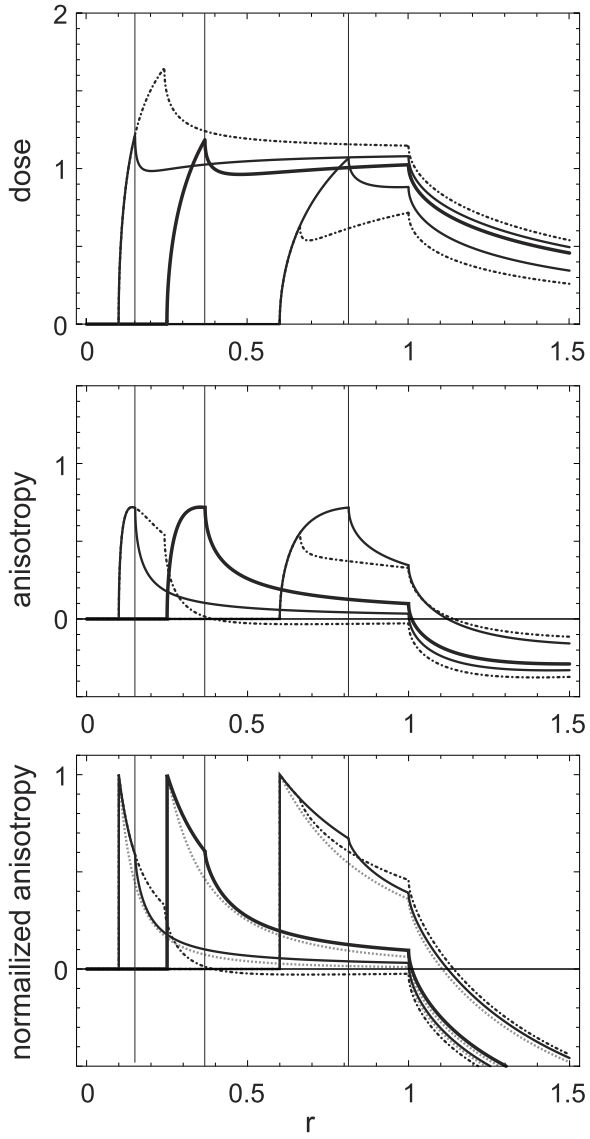

FIG. 5. Adaptation and its correlation with anisotropy. Dose, anisotropy, and normalized anisotropy are shown from top to bottom. Thick solid line: original plan. Thin solid lines: plans adapted according to 2-Step rules. Dashed-dotted lines: adaption using linear fluence warping. Vertical lines: outer border of $S2$-segment: middle–original, left (right) adapted to decreased (increased) OAR radius according to 2-Step rules. Dotted lines: ideal (Brahme) solution–normalized anisotropy only.

[0.25;0.00] → [0.038;2.84], [0.25;0.05] → [0.113;1.03], [0.25;0.10] → [0.172;0.66],
[0.60;0.00] → [0.030;3.60], [0.60;0.05] → [0.103;1.25], [0.60;0.10] → [0.161;0.79].
The mean dose to the PTV was normalized to 1. The calculations were performed with a rectangular beam profile.

Figure 3 depicts the non-zero component of the anisotropy vector on the line of sight and the related normalized anisotropy for both Brahme and 2-Step cases along the radius of the PTV-OAR-configuration. The second anisotropy component was zero because of cylindrical symmetry of the chosen irradiation techniques. As for Brahme's solution the dose to the PTV was always 1, also the anisotropy did not exceed the value of 1 for the tangent point. In the fluence distribution, at R_{OAR} the fluence was infinite, see Fig. 3. All doses at $r = R_{OAR}$ came from the tangential irradiation only, i.e., from a single definite gantry angle. For 2-Step, anisotropy increased above 1, as the dose was normalized to the mean dose of the PTV and a dose hot spot could occur in the near-to-OAR area of dominating tangential irradiation. Normalized anisotropy, however, was more stable: its maximum marked the beginning of the dose gradient and as such corresponded to OAR radius or smaller, if dose gradient started inside the OAR. Such a maximum also existed for the 2-Step technique for the same reason: at the border of the OAR only a tangential dose contribution at a single moment occurred—generated, however, by a vanishingly

smaller dose. Thus for 2-Step, anisotropy increased beginning at R_{OAR}, and for small gaps between OAR and PTV, reached its maximum for the narrow second step $S2$ segments at their outer border. A representation of the absolute value of anisotropy depicted as third dimension above a CT slice always resembled a volcano around the OAR, with the OAR-region as its crater. At maximal OAR sparing normalized anisotropy had a maximum of $A_n = 1$: PTV dose close to OAR came only from tangential irradiation. If OAR was not necessarily to be spared as much as possible, additional dose to the OAR was allowed. If additional contribution to OAR dose and its neighborhood was isotropic, anisotropy A and normalized anisotropy A_n decreased according to Eq. (2) (Fig. 4). If additional contribution to OAR dose was anisotropic, the anisotropy increased in the direction of anisotropic contribution due to linearity. In this direction the normalized anisotropy remained constant and decreased in other direction according to Eq. (2). The "volcano" lost its cylindrical symmetry. Anisotropy and normalized anisotropy inside the OAR increased. Thus, the maximal height of normalized anisotropy around the OAR reflected the importance of OAR-sparing.

Note also in Fig. 3 that

- for radii exceeding the PTV, the non-zero anisotropy vector component dropped below 0 and the normalized form approaches -1 for $r \to \infty$;
- increasing of the PTV-OAR gap led to the broadening of the "anisotropy wall";
- normalized anisotropy for 2-Step and Brahme solutions differed only to a small degree.

3.B. Anisotropy for different beam profiles and isotropic dose contributions (simple beam model and geometry)

To evaluate the influence of beam profiles, a trapezoid profile was chosen with penumbra of 0.03 and 0.06 (Fig. 4). An isotropic dose contribution of 10% was assumed in addition to model long-range scatter. The 2-Step plan was optimized assuming a PTV-OAR gap of 0.05 and an OAR radius of 0.25 (other parameters were the same as in Sec. 3.A). The dose distribution of the original plan developed the desired dose plateau between the inner PTV radius of 0.3 and the outer radius of 1.0, especially using more realistic beams with a penumbra. Anisotropy was only slightly affected by beam profile, except a lowering of the maximum and a minor smearing out. Pure trapezoid profiles shifted the peak of normalized anisotropy inside the OAR to the start point of the dose gradient. This effect was smeared in more realistic beam models with additional isotropic background, which contributes mainly to the denominator of Eq. (2).

Additional isotropic background inhibited beam profile driven shift of normalized anisotropy (Fig. 4) and resulted in a leveled anisotropy peak, which was only marginally shifted in dependence of beam profile.

3.C. Adaptation and anisotropy parameters (simple beam model and geometry)

The adaptation of a 2-Step plan was performed for a situation [OAR-radius 0.25; gap width 0.05] → [2-Step segment width 0.113; segment weight 1.03], for a decreased OAR radius of 0.1 and an increased OAR-radius of 0.6 (Fig. 5). A rectangular beam profile was chosen. The weight of the $S2$-segments was kept constant (1.03), only the width was changed, as it is required for MU-preserving adaptation. For the 2-Step adaptation method, a dose plateau was retained in spite of the considerable changes of the OAR-radius by a factor of 2 or more. Pure fluence adaptation, based on linear interpolation of a grid spanned over the BEV projections of OAR and PTV resulted in severe under or overdosage in the PTV as predicted.[8] Note that the features of normalized anisotropy distribution can be identified (maximum, width at half height) which are closely correlated with the positions of inner and outer borders of $S2$ segments adapted to a new OAR radius (Fig. 5, vertical lines).

3.D. Examples (realistic beam, patient model and plans)

Figure 6 shows anisotropy for two inflated rectum cases (light blue), the first laterally and ventrally (a), the second only laterally (b) with respect to the original plan (dark blue). The

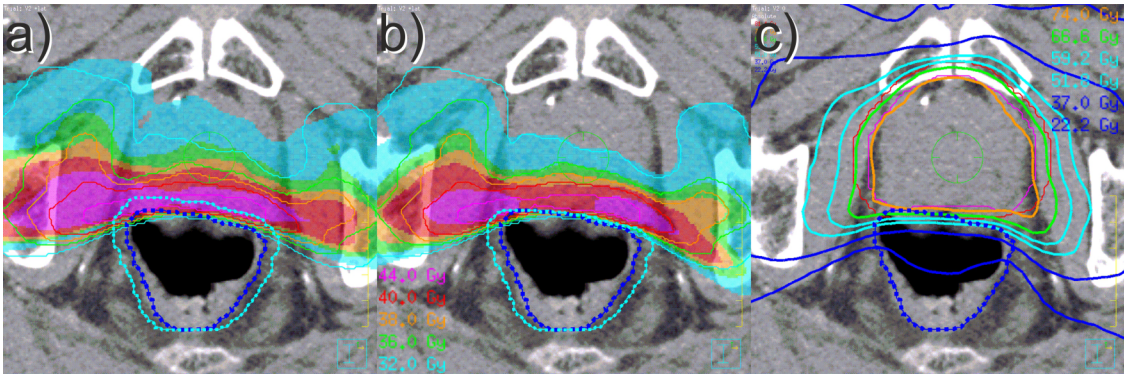

FIG. 6. VMAT prostate irradiation with rectal sparing (dark blue, dotted). Rectum inflated (light blue, dotted) ventral-lateral (a) or only lateral (b). Absolute value of anisotropy vector of Eq. (1) in (a) and (b) for original plan (lines) and the reoptimized plan for inflated rectum (colorwash). Right side (c): Dose distribution of the original plan.

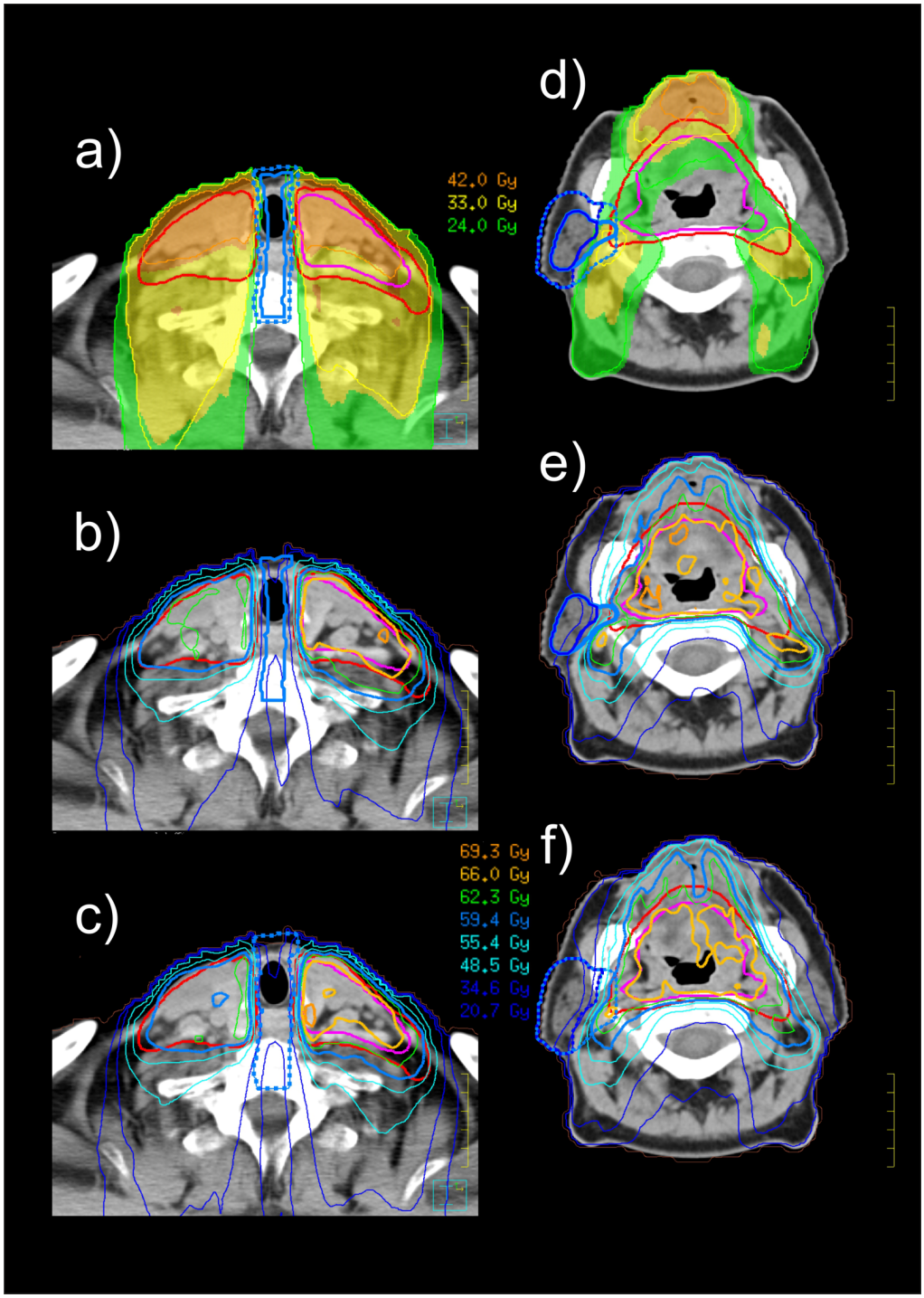

FIG. 7. Head and neck case; left side [(a)–(c)] lymph drainage region; right side [(d)–(f)] parotid gland area. OAR (blue lines): pre- (thick, continuous line) and post inflation (thick, dotted). Iso-anisotropy (a) + (d): lines: primary plan, colorwash: reoptimized to inflated right parotid. (b) + (e) Dose distribution of the original VMAT plan. (c) + (f) Dose distribution reoptimized to inflated right parotid.

anisotropy distribution of the original plan is shown as colored lines; the anisotropy distribution for the changed geometry is shown in colorwash. Lateral increase of OAR leads to the disproportionately high lateral increase of high level iso-anisotropy area near the OAR, lateroventral increase similar to a disproportionate increase of high level iso-anisotropy area in ventral direction. Thus, at least qualitatively, the anisotropy shows the behavior similar to that of $S2$-segments in 2-Step adaptation,[8] corresponding to DC > 1.

Figure 7 depicts a selection of head and neck slices for a patient. Similarly, the anisotropy of Eq. (1) was calculated (a) + (d) for the original VMAT plan (lines) and the reoptimized plan (colorwash). The related dose distributions are shown as isodoses: (b) + (e)–original plan and (c) + (f)–new plan. At the left side [(a)–(c)], a characteristic slice from the lymph drainage area is presented. Anisotropy increases overall in the PTV, when the spared central area is inflated. At the right side [(d)–(f)], a slice across the parotid glands is depicted.

Again, near the inflated parotid the iso-anisotropy area shows a disproportionally high increase outward, whereas at the unmodified side, anisotropy changes only slightly.

4. DISCUSSION

Anisotropy [Eqs. (1) and (2)] can be defined for any IMRT/IMAT/VMAT plan. The small differences between normalized anisotropy of 2-Step and Brahme solutions suggest a sort of universality of normalized anisotropy, perhaps some independence from irradiation technique—a hypothesis to be tested.

For the simplified cases, the peak of normalized anisotropy indicates the position of the OAR border. Qualitatively this can also be seen for the clinical cases, as long as only one OAR is nearby. For multiple OARs, a superposition can be observed [parotids and spinal cord, Fig. 7(d)] or a preferred irradiation direction can lead to high anisotropy over all the PTV [lymph drainage area, Fig. 7(a)]. Nevertheless, also for patient cases, the need of additional tangential dose contributions can be correlated with the anisotropy. As the change in the anisotropy distribution shows, for the changed geometry, similar to the 2-Step adaptation algorithm, the width of the area of tangential, nonisotropic dose contributions (iso-anisotropy area) increases quicker than the OAR radius.

The height of the anisotropy peak around OAR automatically accounts for the power of OAR sparing, the width of this peak seems to correlate with 3D relationships between PTV and OAR in the corresponding CT layer, characterized for the purposes of adaptation by the radius of OAR and the width of the gap between OAR and PTV, normalized to PTV radius. Independently of the irradiation technique, increasing of OAR radius causes a broadening of the anisotropy peak around OAR just as it is required for second step ($S2$) segments in the case of 2-Step adaptation.[8,16] Thus, the anisotropy of Eqs. (1) and (2) can help identify tangential-to-OAR parts of arbitrary IMRT or IMAT/VMAT segments. If projected into BEV, anisotropy should provide a special warping grid for such segments which would correctly take changed PTV-OAR relationships into account.

Finally, further fields of research arise. First, the 3D deformation of the anisotropy near the deformed OAR has to be explored. Second, projecting of the deformed anisotropy into BEV has to be addressed. Obviously, only (normalized) anisotropy in or near to the PTV is interesting. (The anisotropy increase far away from PTV reflects the trivial fact that single beams dominate there.) The authors assume that for BEV warping the anisotropy vector component along the beam direction should be considered, as the tangential components of anisotropy should then be more clearly visible, but this point must be investigated in more detail. Third, the algorithms for identification of relevant leaf pairs and their transformation in BEV have to be developed.

Provided these investigations have been successful, the adaptation process would have the following steps as described in the Introduction:

(1) Optimization of arbitrary IMRT or VMAT
   (a) and calculation of the related anisotropy vector field,
   (b) projection of the vectors in the BEV,
   (c) relation to the beams segments and structures,
(2) Contouring of daily target and OARs in actual CBCT or MR
   (a) warping of the anisotropy in 3D,
   (b) projection of contours and anisotropy vector field in BEV,
   (c) adaptation of anisotropy vector field to a new geometry, warping of the beam shapes along with projected contours, and anisotropy vector field. The exact form of the anisotropy projection (e.g., anisotropy vector component along the beam direction, projected into BEV) is a matter of further investigation.
(3) Plausibility checks and dose accumulation

In case all these developments are advanced enough, the extension of anisotropy definition into spherical domain for non-coplanar IMRT beam arrangements[17] can be considered.

5. CONCLUSION

The first results suggest that distribution of anisotropy defined in Eq. (1) behaves under changed patient geometry similar to the segments of 2-Step IMRT and VMAT plans, which saturate the dose in the PTV areas adjacent to OARs. Therefore, the authors see a good chance to generalize 2-Step adaptation rules for the case of arbitrary IMRT/VMAT plans incorporating some form of BEV projection of proposed anisotropy distribution into a warping grid.

Further work is needed to investigate its properties for several realistic cases of IMRT and VMAT planning. Then, the behavior of the anisotropy is to be analyzed in more detail for real deformations of organs. Finally, the identification of leaf positions that lead to OAR-tangential dose contributions is to be performed and an algorithm for leaf adaption in dependence of anisotropy deformation has to be developed.

ACKNOWLEDGMENTS

The authors thank Henrik Schachner for many productive discussions and Anne Richter for help with PINNACLE3 handling.

CONFLICT OF INTEREST DISCLOSURE

The authors have no COI to report.

[a]Author to whom correspondence should be addressed. Electronic mail: Bratengeie_K@ukw.de

[1]K. Bratengeier, M. Guckenberger, J. Meyer, G. Muller, L. Pfreundner, F. Schwab, and M. Flentje, "A comparison between 2-step IMRT and conventional IMRT planning," Radiother. Oncol. **84**, 298–306 (2007).

[2]J. Wilbert, K. Baier, C. Hermann, M. Flentje, and M. Guckenberger, "Accuracy of real-time couch tracking during 3-dimensional conformal radiation therapy, intensity modulated radiation therapy, and volumetric modulated arc therapy for prostate cancer," Int. J. Radiat. Oncol., Biol., Phys. **85**, 237–242 (2013).
[3]T. Ravkilde, P. J. Keall, C. Grau, M. Hoyer, and P. R. Poulsen, "Fast motion-including dose error reconstruction for VMAT with and without MLC tracking," Phys. Med. Biol. **59**, 7279–7296 (2014).
[4]C. Men, H. E. Romeijn, X. Jia, and S. B. Jiang, "Ultrafast treatment plan optimization for volumetric modulated arc therapy (VMAT)," Med. Phys. **37**, 5787–5791 (2010).
[5]Q. J. Wu, D. Thongphiew, Z. Wang, B. Mathayomchan, V. Chankong, S. Yoo, W. R. Lee, and F. F. Yin, "On-line re-optimization of prostate IMRT plans for adaptive radiation therapy," Phys. Med. Biol. **53**, 673–691 (2008).
[6]R. Mohan, X. Zhang, H. Wang, Y. Kang, X. Wang, H. Liu, K. K. Ang, D. Kuban, and L. Dong, "Use of deformed intensity distributions for on-line modification of image-guided IMRT to account for interfractional anatomic changes," Int. J. Radiat. Oncol., Biol., Phys. **61**, 1258–1266 (2005).
[7]W. Crijns, G. Defraene, H. Van Herck, T. Depuydt, K. Haustermans, F. Maes, and F. Van den Heuvel, "Online adaptation and verification of VMAT," Med. Phys. **42**, 3877–3891 (2015).
[8]K. Bratengeier, M. Oechsner, and M. Gainey, "Methods for monitor-unit-preserving adaptation of intensity modulated arc therapy techniques to the daily target—A simple comparison," Med. Phys. **39**, 713–720 (2012).
[9]K. Bratengeier, M. Gainey, O. A. Sauer, A. Richter, and M. Flentje, "Fast intensity-modulated arc therapy based on 2-step beam segmentation," Med. Phys. **38**, 151–165 (2011).
[10]M. Gainey, K. Holubyev, and K. Bratengeier, "Towards routine 2-step based IMRT/IMAT treatment planning in the clinic," J. Bioinf. Biol. Eng. **2**, 1–12 (2014), see www.academicpub.org/DownLoadPaper.aspx?PaperID=15313.
[11]K. Bratengeier, B. Polat, M. Gainey, P. Grewenig, J. Meyer, and M. Flentje, "Is *ad-hoc* plan adaptation based on 2-step IMRT feasible?," Radiother. Oncol. **93**, 266–272 (2009).
[12]K. Holubyev, K. Bratengeier, M. Gainey, B. Polat, and M. Flentje, "Towards automated on-line adaptation of 2-step IMRT plans: Quasimodo phantom and prostate cancer cases," Radiat. Oncol. **8**, 263 (12pp.) (2013).
[13]K. Holubyev, M. Gainey, K. Bratengeier, B. Polat, and M. Flentje, "Generation of prostate IMAT plans adaptable to the inter-fractional changes of patient geometry," Phys. Med. Biol. **59**, 1947–1962 (2014).
[14]A. Brahme, J. E. Roos, and I. Lax, "Solution of an integral equation encountered in rotation therapy.," Phys. Med. Biol. **27**, 1221–1229 (1982).
[15]K. Bratengeier, "2-step IMAT and 2-step IMRT: A geometrical approach," Med. Phys. **32**, 777–785 (2005).
[16]K. Bratengeier, "2-step IMAT and 2-step IMRT in three dimensions," Med. Phys. **32**, 3849–3861 (2005).
[17]K. Bratengeier and K. Holubyev, "Characteristics of non-coplanar IMRT in the presence of target-embedded organs at risk," Radiat. Oncol. **10**, 207 (13pp.) (2015).